Accelerometer Bias Calibration Using Attitude and Angular Velocity Information

Zhengshi Yu*

Beijing Institute of Technology, Beijing, China, 100081

John L. Crassidis†

University at Buffalo, State University of New York, Amherst, NY, 14260-4400

For accurate inertial navigation, an accelerometer should be calibrated before usage to reduce error accumulation. However, if limited or no translational observations are available, which is a technical challenge for many applications such as Mars exploration missions, the accelerometer calibration must be conducted using alternative approaches. This paper proposes a novel accelerometer calibration method using attitude and angular velocity information only. In the algorithm, angular acceleration is measured by a gyro-free inertial navigation scheme to propagate the attitude dynamics and kinematics. The attitude, angular velocity, and accelerometer biases are regarded as states of the calibration system. An extended Kalman filter is employed to estimate the states using attitude and angular velocity outputs from the attitude determination system. A discrete-time model and corresponding covariance matrix are derived. Also the observability of the calibration system is analyzed. It is shown that the biases are not all observable; only a linear combination of them is observable. Therefore, a recalculation process is introduced to improve the calibration performance. Furthermore, the covariance intersection method is used to determine a consistent estimator. Simulation results demonstrate that the proposed method can effectively calibrate accelerometers with high accuracy and improve the performance of the attitude estimates.

*Graduate Student, School of Aerospace Engineering. Email: yuzhengshi@gmail.com.

†CUBRC Professor in Space Situational Awareness, Department of Mechanical & Aerospace Engineering. Email: johnc@buffalo.edu, Fellow AIAA.

Nomenclature

A	=	direction cosine matrix from inertial reference frame to body frame
$\boldsymbol{a}$	=	acceleration, m/s^2
$\boldsymbol{b}$	=	vector of accelerometer biases, m/s^2
$\boldsymbol{f}$	=	non-gravitational acceleration, m/s^2
$\tilde{\boldsymbol{f}}$	=	accelerometer measurement, m/s^2
$\boldsymbol{g}$	=	gravitational acceleration, m/s^2
H	=	sensitivity matrix
$\boldsymbol{h}$	=	measurement equation
J	=	moment of inertia, kg-m^2
O	=	observability matrix
P	=	covariance of state vector
Q	=	covariance of the process noise
$\boldsymbol{q}$	=	quaternion
R	=	position matrix of accelerometers
$\boldsymbol{r}$	=	position vector of accelerometer, m
T	=	direction cosine matrix from accelerometer reference frame to body frame
$\boldsymbol{u}_c$	=	control acceleration, m/s^2
$\boldsymbol{x}$	=	state vector of calibration system
$\boldsymbol{y}$	=	vector of observations
$\boldsymbol{\delta\vartheta}$	=	attitude error, rad
$\boldsymbol{\nu}$	=	measurement noise
$\boldsymbol{\eta}$	=	white noise of accelerometer
σ	=	standard deviation of noise
Φ	=	error-state transition matrix
$\boldsymbol{\omega}$	=	angular velocity, rad/s
$\dot{\boldsymbol{\omega}}$	=	angular acceleration, rad/s^2

I. Introduction

Many applications require the use of dead reckoning for navigation purposes, including, but not limited to, spacecraft, air, sea, automotive, pedestrian, and robotic systems navigation. The Mars landing problem is an example of a spacecraft navigation application.

To date, all Mars landing vehicles rely on some kind of dead reckoning navigation system using an Inertial Measurement Unit (IMU) during the entry phase.[1] Because the duration of entry phase is only about four to six minutes, high enough accuracy can be achieved as long as the initial entry states are accurately determined. The drift and/or bias in the gyro and accelerometer, which may accumulate with time, are the main contributors to the navigation accuracy.[2] Therefore, accurate calibration of the gyros and accelerometers is indispensable before Mars entry. Because no frequent attitude or orbit maneuvers are conducted during the Mars approach phase, a relatively stable flight condition can be achieved. This makes the Mars approach phase an ideal period to perform gyro and accelerometer calibration.

The attitude and translation estimation systems, which use different kinds of sensors, are usually separated. For the attitude estimation system, star trackers can be used to calibrate the gyros with high accuracy. On the other hand, for the translation estimation system, infrequent navigation information, such as limited ground-based tracking used for position and velocity determination, makes the calibration of the accelerometers much more difficult than the attitude estimation system. Therefore, it is useful to develop an accelerometer calibration method using attitude sensors. From an estimation theory point of view, if a relationship between the accelerometer biases, the vehicles's attitude, and the angular velocity can be found, then the aforementioned accelerometer calibration problem can be solved using a filtering algorithm.

The concept of determining the attitude kinematics of a rigid body based on accelerometers has been vigorously investigated in the past. References 3 and 4 proposed the initial idea of measuring angular velocity without using gyros, and introduced the preliminary scheme of an inertial navigation using only accelerometers. Reference 5 further improved previous research by proposing two schemes including six and nine accelerometers. In this work it is concluded that if the configuration of accelerometers can be properly chosen, then the minimum number of linear accelerometers to determine the angular acceleration directly, without involving angular velocity terms, is nine. These results also laid the foundation of the following investigations. The stability of the approach in Ref. 5 is discussed in Ref. 6. Furthermore, Ref. 7 uses the six-accelerometer approach to compute the angular acceleration, and integrated the attitude dynamics to achieve attitude determination. Also using six accelerometers, Ref. 8 proposes a strapdown and gyro-free inertial navigation approach which computes the angular acceleration and location of a vehicle, and presents a theoretical minimum workable accelerometer configuration.

Recently, more attention has been paid to improving the performance of a gyro-free inertial navigation system. Reference 9 develops an IMU-based approach with twelve accelerometers which can directly determine the angular velocity, and determine the location and direction of the accelerometers by minimizing the numerical conditioning of a coefficient

matrix. In Refs. 10 and 11 a sufficient condition is presented to determine the feasibility of the configuration of the accelerometers, and to analyze the effects of accelerometer location and orientation errors. Reference 12 investigates the configuration of a gyro-free IMU with noisy accelerometer measurements in order to obtain the best observability. Furthermore, a multi-position calibration method to determine the orientation and position errors of accelerometers is shown in Ref. 13.

On the other hand, very little research has been conducted on how to calibrate the biases of accelerometers, which may have a major impact on the navigation accuracy. The use of star trackers and a gravity field gradiometer to calibrate six accelerometers is shown in Ref. 14. In the algorithm, the attitude of the spacecraft is determined by a star tracker which is then used to determine the angular velocity and acceleration by employing a quadratic fit. Then based on a model of the accelerometer output, the biases can be estimated by a least squares method. However, even though the attitude can be accurately determined by a star tracker, the computation of the angular velocity and acceleration might introduce additional errors which may reduce the accuracy of the bias estimation. Reference 15 also introduces a calibration approach using a gyro-free IMU. Given the vehicle's angular velocity and acceleration, the positions, orientations and biases of the accelerometers can be determined by solving a least squares problem. Then the angular velocity and acceleration are further estimated using an unscented Kalman filter. Nevertheless, the accuracy of the calibration method heavily relies on the number of accelerometers and on the accuracy of the attitude estimates.

In order to overcome such shortcomings of previous calibration methods, this paper investigates the possibility of accelerometer calibration using only attitude and angular velocity information. It is also the first known attempt to calibrate the accelerometer biases based on a filtering method. This is a valuable issue for applications with limited translational observations too. From the output model of multiple triaxial accelerometers, the angular acceleration containing the information of accelerometer biases can be measured and used to propagate the attitude dynamics and kinematics. Then the information of attitude and angular velocity from the attitude determination system can be used to estimate the biases of the accelerometers, as well as other states such as attitude and angular velocity using a filtering algorithm. Based on an observability analysis, a recalculation process is added to improve the calibration performance.

The content of this paper is organized as follows. First, the accelerometer output model, attitude kinematics, and observation models are introduced in Section II. Then the new calibration method, including an extended Kalman filter (EKF) and a recalculation process are developed in Section III, which is the main part of the paper. Also, an observability analysis is conducted. Next, in Section IV an accelerometer calibration procedure is considered where

three accelerometers are calibrated based on the proposed method. The optimality of the calibration system is also analyzed using a covariance intersection method. Furthermore, the accuracy of the proposed calibration method is discussed.

II. Underlying Kinematics

A. Accelerometer Output Model

In this section, the basic principle of a gyro-free IMU is reviewed, and the output model for the accelerometers is also introduced. In theory, in order to measure the angular velocity and acceleration terms, multiple accelerometers mounted at different positions on a vehicle, regarded as a rigid body, are required. Considering n triaxial accelerometers at points $P_1, \ldots, P_n$, the acceleration of each point is given by

$$\boldsymbol{a}_i = \boldsymbol{a}_c + \dot{\boldsymbol{\omega}} \times \boldsymbol{r}_i + \boldsymbol{\omega} \times (\boldsymbol{\omega} \times \boldsymbol{r}_i)\,,\ i = 1, \ldots, n \tag{1}$$

where $\boldsymbol{a}_c$ is the total acceleration including the gravity, $\boldsymbol{\omega}$ and $\dot{\boldsymbol{\omega}}$ are the angular velocity and angular acceleration of the vehicle, respectively, and $\boldsymbol{r}_i$ indicates the position vector of P_i relative to the mass center. For a spacecraft, the acceleration exerted at the mass center can be divided into a gravitational term $\boldsymbol{g}$ and a control term $\boldsymbol{u}_c$, determined from the control system. Similarly, the acceleration at point P_i also contains the gravitational term $\boldsymbol{g}_i$ and the non-gravitational term $\boldsymbol{f}_i$, which can be measured by triaxial accelerometer. Because the size of a spacecraft is commonly not large and the estimation convergence time is fast, the gravity gradient term can be typically ignored, which leads to $\boldsymbol{g}_i = \boldsymbol{g}$. Therefore, the relationship between the output of the accelerometer and the angular velocity and acceleration can be established through

$$T_i^b\, \boldsymbol{f}_i = \boldsymbol{u}_c + \left(\Omega^2 + \dot{\Omega}\right) \boldsymbol{r}_i \equiv \boldsymbol{u}_c + \bar{\Omega} \boldsymbol{r}_i \tag{2}$$

In this equation, T_i^b refers to the direction cosine matrix that takes the accelerometer's reference frame to the body frame. Also, the antisymmetrical matrix Ω is given by

$$\Omega = \begin{bmatrix} 0 & -\omega_z & \omega_y \\ \omega_z & 0 & -\omega_x \\ -\omega_y & \omega_x & 0 \end{bmatrix}$$

where ω_x, ω_y and ω_z are components of $\boldsymbol{\omega}$. Furthermore, Ω^2 and $\dot{\Omega}$ represent the square and derivative of Ω.

The principle of the gyro-free IMU is shown in Figure 1, where O_I is the inertial frame,

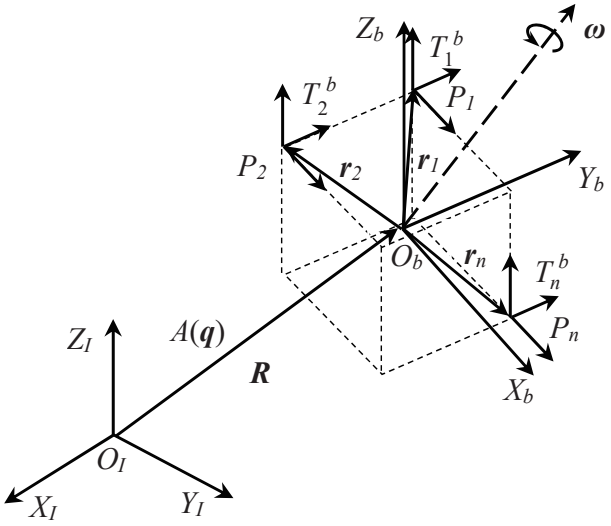

Figure 1. Principle of a Gyro-Free IMU

and O_b is the body frame. The accelerometer measurements are modeled by

$$\tilde{\boldsymbol{f}}_i = \boldsymbol{f}_i + \boldsymbol{b}_i + \boldsymbol{\eta}_{vi} \tag{3a}$$

$$\dot{\boldsymbol{b}}_i = \boldsymbol{\eta}_{ui} \tag{3b}$$

where $\tilde{\boldsymbol{f}}_i$ is the output of accelerometer, $\boldsymbol{b}_i$ is the bias, and $\boldsymbol{\eta}_{vi}$ and $\boldsymbol{\eta}_{ui}$ are the corresponding measurement and process noises modeled by uncorrelated Gaussian white-noises satisfying

$$E\left\{\boldsymbol{\eta}_{vi}(t)\,\boldsymbol{\eta}_{vi}^T(\tau)\right\} = \sigma_{vi}^2\delta(t-\tau)\,I_3 \tag{4a}$$

$$E\left\{\boldsymbol{\eta}_{ui}(t)\,\boldsymbol{\eta}_{ui}^T(\tau)\right\} = \sigma_{ui}^2\delta(t-\tau)\,I_3 \tag{4b}$$

where $\delta(t-\tau)$ is the Dirac delta function and I_3 is a 3×3 identity matrix. It is assumed here that the spectral densities of $\boldsymbol{\eta}_{vi}$ and $\boldsymbol{\eta}_{ui}$ are the same on all axes, so that $\sigma_{vi} = \sigma_v$ and $\sigma_{ui} = \sigma_u$. Discrete-time accelerometer measurements can be simulated by[16]

$$\tilde{\boldsymbol{f}}_{i_{k+1}} = \boldsymbol{f}_{i_{k+1}} + \frac{1}{2}(\boldsymbol{b}_{i_{k+1}} + \boldsymbol{b}_{i_k}) + \left(\frac{\sigma_v^2}{\Delta t} + \frac{1}{12}\sigma_u^2\,\Delta t\right)^{1/2}\mathbf{N}_{vi_k} \tag{5a}$$

$$\boldsymbol{b}_{i_{k+1}} = \boldsymbol{b}_{i_k} + \sigma_u\,\Delta t^{1/2}\mathbf{N}_{ui_k} \tag{5b}$$

where the subscript k denotes the k^{th} time-step, and $\mathbf{N}_{vi_k}$ and $\mathbf{N}_{ui_k}$ are zero-mean Gaussian white-noise processes with covariance each given by the identity matrix.

Considering n triaxial accelerometers, the accelerometer model is given using an appended

matrix form:

$$\bar{\Omega}R = \tilde{F} - B - V \tag{6}$$

where $R = [\boldsymbol{r}_1, \ldots, \boldsymbol{r}_n]$, $\tilde{F} = \left[T_1^b \tilde{\boldsymbol{f}}_1 - \boldsymbol{u}_c, \ldots, T_n^b \tilde{\boldsymbol{f}}_n - \boldsymbol{u}_c\right]$, $B = \left[T_1^b \boldsymbol{b}_1, \ldots, T_n^b \boldsymbol{b}_n\right]$, and $V = \left[T_1^b \boldsymbol{\eta}_{v1}, \ldots, T_n^b \boldsymbol{\eta}_{vn}\right]$. If more than three accelerometers are used, then the matrix $\bar{\Omega}$ can be computed using

$$\begin{aligned} \bar{\Omega} &= \tilde{F}R^* - BR^* - VR^* \\ &\equiv \tilde{\bar{\Omega}} - BR^* - VR^* \end{aligned} \tag{7}$$

where R^* is the pseudoinverse of R satisfying $R^* = R^T \left(RR^T\right)^{-1}$.

The negative diagonal elements of $\bar{\Omega}$ are only related to the angular velocity. Measurement noise from the accelerometers may cause a violation of negativeness though. Therefore, the angular velocity cannot be directly determined using only Eq. (7). However, the angular acceleration can be calculated by defining

$$T_i^b = \left[\left(\boldsymbol{T}_{i1}^b\right)^T, \left(\boldsymbol{T}_{i2}^b\right)^T, \left(\boldsymbol{T}_{i3}^b\right)^T\right]^T \tag{8a}$$

$$R^* = \begin{bmatrix} R_{11}^* & R_{12}^* & R_{13}^* \\ \vdots & \vdots & \vdots \\ R_{n1}^* & R_{n2}^* & R_{n3}^* \end{bmatrix} \tag{8b}$$

$$\Gamma_i = \left[R_{i2}^* \left(\boldsymbol{T}_{i3}^b\right)^T - R_{i3}^* \left(\boldsymbol{T}_{i2}^b\right)^T, R_{i3}^* \left(\boldsymbol{T}_{i1}^b\right)^T - R_{i1}^* \left(\boldsymbol{T}_{i3}^b\right)^T, R_{i2}^* \left(\boldsymbol{T}_{i1}^b\right)^T - R_{i1}^* \left(\boldsymbol{T}_{i2}^b\right)^T\right]^T \tag{8c}$$

where $\left(\boldsymbol{T}_{ij}^b\right)^T$ is the j^{th} column of $\left(T_i^b\right)^T$. The angular acceleration is given by

$$\begin{aligned} \dot{\boldsymbol{\omega}} &= \frac{1}{2}\begin{bmatrix} \bar{\Omega}_{32} - \bar{\Omega}_{23} \\ \bar{\Omega}_{13} - \bar{\Omega}_{31} \\ \bar{\Omega}_{21} - \bar{\Omega}_{12} \end{bmatrix} \\ &= \frac{1}{2}\begin{bmatrix} \tilde{\bar{\Omega}}_{32} - \tilde{\bar{\Omega}}_{23} \\ \tilde{\bar{\Omega}}_{13} - \tilde{\bar{\Omega}}_{31} \\ \tilde{\bar{\Omega}}_{21} - \tilde{\bar{\Omega}}_{12} \end{bmatrix} - \frac{1}{2}\sum_{i=1}^{n} \Gamma_i \boldsymbol{b}_i - \frac{1}{2}\sum_{i=1}^{n} \Gamma_i \boldsymbol{\eta}_{vi} \\ &\equiv \tilde{\dot{\boldsymbol{\omega}}} - \frac{1}{2}\sum_{i=1}^{n} \Gamma_i \boldsymbol{b}_i - \frac{1}{2}\sum_{i=1}^{n} \Gamma_i \boldsymbol{\eta}_{vi} \end{aligned} \tag{9}$$

Equation (9) is the model for the accelerometer output. The vector of accelerometer biases is defined by $\boldsymbol{b} = \left[\boldsymbol{b}_1^T, \ldots, \boldsymbol{b}_n^T\right]^T$.

B. Attitude Kinematics

In order to calibrate the accelerometers based on attitude and angular velocity information, the relationship between the accelerometer biases and the attitude of the vehicle also needs to be found, which relies on the attitude kinematics model of the vehicle. In order to avoid potential singularity issues caused by Euler angles, the quaternion $\boldsymbol{q} \equiv \left[\boldsymbol{q}_{1:3}^T, q\right]^T$ is used to describe the attitude of the vehicle. Here $\boldsymbol{q}_{1:3} = [q_1, q_2, q_3]^T$ is the vector part of the quaternion, while q is the scalar part. The attitude kinematics of the vehicle can be modeled by[16]

$$\dot{\boldsymbol{q}} = \frac{1}{2}\begin{bmatrix}\boldsymbol{\omega}\\ 0\end{bmatrix} \otimes \boldsymbol{q} = \frac{1}{2}\Xi(\boldsymbol{q})\,\boldsymbol{\omega} \tag{10}$$

where $\otimes$ denotes quaternion multiplication[17] and the matrix $\Xi(\boldsymbol{q})$ is defined by

$$\Xi(\boldsymbol{q}) = \begin{bmatrix}[\boldsymbol{q}_{1:3}\times] + qI_3\\ -\boldsymbol{q}_{1:3}^T\end{bmatrix} \tag{11}$$

and $[\boldsymbol{q}_{1:3}\times]$ is the standard cross product matrix.

Furthermore, a three-component column state vector $\boldsymbol{\delta\vartheta}$ is used in the EKF for the representation of the attitude errors. The quaternion error defined in the body frame is thus approximated by $\boldsymbol{\delta q} \approx \left[\frac{1}{2}\boldsymbol{\delta\vartheta}^T, 1\right]^T$, and the relationship between the true and estimated quaternions is given by

$$\boldsymbol{q} = \boldsymbol{\delta q} \otimes \hat{\boldsymbol{q}} \approx \hat{\boldsymbol{q}} + \frac{1}{2}\Xi(\hat{\boldsymbol{q}})\,\boldsymbol{\delta\vartheta} \tag{12}$$

The propagation of the error quaternion satisfies

$$\begin{aligned}\boldsymbol{\delta\dot{q}} &= \frac{1}{2}\left(\begin{bmatrix}\boldsymbol{\omega}\\ 0\end{bmatrix} \otimes \boldsymbol{\delta q} - \boldsymbol{\delta q} \otimes \begin{bmatrix}\hat{\boldsymbol{\omega}}\\ 0\end{bmatrix}\right)\\ &= -\begin{bmatrix}[\hat{\boldsymbol{\omega}}\times]\,\boldsymbol{\delta q}_{1:3}\\ 0\end{bmatrix} + \frac{1}{2}\begin{bmatrix}\boldsymbol{\omega} - \hat{\boldsymbol{\omega}}\\ 0\end{bmatrix}\end{aligned} \tag{13}$$

where $\boldsymbol{\delta q}_{1:3}$ is a vector made up of the first three components of $\boldsymbol{\delta q}$. Therefore, the propagation of $\boldsymbol{\delta\vartheta}$ is defined by[16]

$$\boldsymbol{\delta\dot{\vartheta}} = -[\hat{\boldsymbol{\omega}}\times]\,\boldsymbol{\delta\vartheta} + \boldsymbol{\omega} - \hat{\boldsymbol{\omega}} \tag{14}$$

The state vector for the calibration system is $\boldsymbol{x} \equiv \left[\boldsymbol{\delta\vartheta}^T, \boldsymbol{\omega}^T, \boldsymbol{b}^T\right]^T$. Equations (3), (9) and (14) describe the continuous-time model of the calibration system.

C. Observation Model

In the algorithm, both attitude and angular velocity information are considered as observations. It is assumed here that full three-axis estimated attitude and angular velocity can be obtained from an attitude determination system. In practice, there are several approaches to estimate the angular velocity and attitude. The most common way is filtering the attitude sensors (e.g. star trackers, Sun sensors, etc.) with gyro measurements to determine the attitude and gyro bias. The angular velocity can be calculated by subtracting the bias from gyro measurements.[18] Another approach is to develop a model-based filter to estimate the attitude and angular velocity only based on attitude sensors.[19] Besides using filtering approaches, it is also possible to estimate the angular velocity directly from the star tracker body measurements based on a least squares method.[20] Instead of using the attitude from an attitude determination system, the raw measurements from attitude sensors can also be used to obtain attitude information.

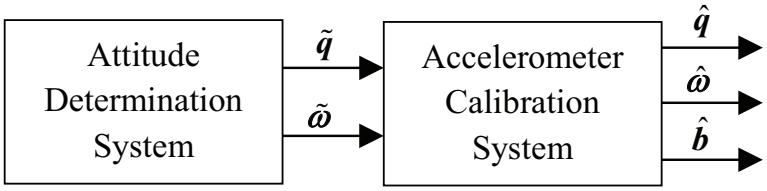

Figure 2. Overall Calibration Approach

The overall approach for the accelerometer calibration process is shown in Figure 2. The attitude determination system provides quaternion and angular velocity outputs, denoted by $\tilde{\boldsymbol{q}}$ and $\tilde{\boldsymbol{\omega}}$, respectively, that are fed into the accelerometer calibration system, which provides estimates of the quaternion, the angular velocity, and the accelerometer biases. As mentioned above there are multiple ways to determine the attitude and angular velocity estimates. The more traditional attitude determination algorithm involves using gyros for the angular velocity, which is the approach used in this work. It should be mentioned that the approach shown in Figure 2 may lead to correlation issues because there are two decentralized filters which estimate the attitude running in parallel, and the attitude sensor measurements are used in both systems. This problem will be addressed later using the covariance intersection approach. Another approach involves determining the angular velocity from attitude reference system (e.g. star tracker) outputs, so that the known source of acceleration can be determined. The angular accelerations can then be derived from Euler's rigid body equations of motion in a torque-free environment. But the accuracy of this approach may depend on how well the inertias are known. The formulation developed here avoids the need to estimate inertias altogether.

Here, the quaternion and angular velocity outputs from the attitude determination system

are considered as observations. The reason is that many modern-day star trackers output a quaternion directly. The measured attitude error can be calculated by

$$\boldsymbol{\delta\tilde{q}} = \tilde{\boldsymbol{q}} \otimes \hat{\boldsymbol{q}}^{-1} \tag{15}$$

where $\hat{\boldsymbol{q}}^{-1}$ is the inverse of the quaternion $\hat{\boldsymbol{q}}$ satisfying $\hat{\boldsymbol{q}}^{-1} = \left[-\hat{\boldsymbol{q}}_{1:3}^T, \hat{q}\right]^T$. The attitude error can be determined by $\boldsymbol{\delta\tilde{\vartheta}} = \frac{1}{2}\boldsymbol{\delta\tilde{q}}_{1:3}$, where $\boldsymbol{\delta\tilde{q}}_{1:3}$ is a vector made up of the first three components of $\boldsymbol{\delta\tilde{q}}$. Therefore the attitude observation can be considered as the attitude error itself, given by

$$\boldsymbol{y}_{\vartheta_k} \equiv \boldsymbol{\delta\tilde{\vartheta}}_k = \boldsymbol{\delta\vartheta}_k + \boldsymbol{\nu}_{\vartheta_k} \tag{16}$$

The observation model for the angular velocity is simply given by

$$\boldsymbol{y}_{\omega_k} \equiv \tilde{\boldsymbol{\omega}}_k = \boldsymbol{\omega}_k + \boldsymbol{\nu}_{\omega_k} \tag{17}$$

Therefore, the observation model can be abbreviated by $\boldsymbol{y}_k = \left[\boldsymbol{y}_{\vartheta_k}^T, \boldsymbol{y}_{\omega_k}^T\right]^T \equiv \boldsymbol{h}\left(\boldsymbol{x}_k\right) + \boldsymbol{\nu}_k$. The full 6×6 measurement covariance R_k of $\boldsymbol{\nu}_k$ can be derived from the error-covariance provided by the attitude determination system. Furthermore, the sensitivity matrix $H_k\left(\hat{\boldsymbol{x}}_k^-\right)$ used in the EKF is given by $H_k\left(\hat{\boldsymbol{x}}_k^-\right) = [I_6, O_{6\times 3n}]$, which leads to $\boldsymbol{h}\left(\hat{\boldsymbol{x}}_k^-\right) = H_k\hat{\boldsymbol{x}}_k^-$.

III. Accelerometer Calibration

A. Discrete-Time Model

Although a continuous-time model has been defined previously, for filtering purposes it is desired to derive a discrete-time model. Based on the continuous-time model of the calibration system, the linearized model is given by

$$\Delta\dot{\boldsymbol{x}}(t) = F(t)\Delta\boldsymbol{x}(t) + G(t)\boldsymbol{\eta}(t) \tag{18}$$

where $\Delta\boldsymbol{x}(t)$ is the linearized state vector associated with $\boldsymbol{x}(t)$, and $\boldsymbol{\eta}\left(t\right)$ is the process noise satisfying $\boldsymbol{\eta}\left(t\right) = \left[\eta_{v1}\left(t\right), \ldots, \eta_{vn}\left(t\right), \eta_{u1}\left(t\right), \ldots, \eta_{un}\left(t\right)\right]^T$, which is a zero-mean Gaussian noise process with spectral density given by $Q(t)$. The matrices $F\left(t\right)$, $G\left(t\right)$ and $Q\left(t\right)$ are

given by

$$F(t) = \begin{bmatrix} -[\hat{\boldsymbol{\omega}}(t)\times] & I_3 & O_{3\times 3n} \\ O_{3\times 3} & O_{3\times 3} & -\frac{1}{2}\Gamma \\ O_{3n\times 3} & O_{3n\times 3} & O_{3n\times 3n} \end{bmatrix} \tag{19a}$$

$$G(t) = \begin{bmatrix} O_{3\times 3n} & O_{3\times 3n} \\ -\frac{1}{2}\Gamma & O_{3\times 3n} \\ O_{3n\times 3n} & I_{3n} \end{bmatrix} \tag{19b}$$

$$Q(t) = \begin{bmatrix} \sigma_v^2 I_{3n} & O_{3n\times 3n} \\ O_{3n\times 3n} & \sigma_u^2 I_{3n} \end{bmatrix} \tag{19c}$$

where $\Gamma = [\Gamma_1, \ldots, \Gamma_n]$. Assuming that $F(t)$ is constant over the sampling interval, a closed-form discrete error-state transition matrix can be derived using a power series approach:

$$\Phi_k = e^{F(t_k)\Delta t} = \sum_{j=0}^{\infty} \frac{\Delta t^j}{j!} F^j(t_k) = \begin{bmatrix} \Phi_{11_k} & \Phi_{12_k} & \Phi_{13_k} \\ O_{3\times 3} & I_3 & -\frac{1}{2}\Delta t\Gamma \\ O_{3n\times 3} & O_{3n\times 3} & I_{3n} \end{bmatrix} \tag{20}$$

where

$$\Phi_{11_k} = \sum_{j=0}^{\infty} \frac{(-1)^j \Delta t^j [\hat{\boldsymbol{\omega}}_k\times]^j}{j!} \tag{21a}$$

$$\Phi_{12_k} = \sum_{j=1}^{\infty} \frac{(-1)^{j-1} \Delta t^j [\hat{\boldsymbol{\omega}}_k\times]^{j-1}}{j!} \tag{21b}$$

$$\Phi_{13_k} = \sum_{j=2}^{\infty} \frac{(-1)^{j-2} \Delta t^j [\hat{\boldsymbol{\omega}}_k\times]^{j-2}}{j!} \left(-\frac{1}{2}\Gamma\right) \tag{21c}$$

It is important to note that the antisymmetric matrix $[\hat{\boldsymbol{\omega}}_k\times]$ has the following identities:

$$[\hat{\boldsymbol{\omega}}_k\times]^{2k+1} = (-1)^k \|\hat{\boldsymbol{\omega}}_k\|^{2k} [\hat{\boldsymbol{\omega}}_k\times] \tag{22a}$$

$$[\hat{\boldsymbol{\omega}}_k\times]^{2k+2} = (-1)^k \|\hat{\boldsymbol{\omega}}_k\|^{2k} [\hat{\boldsymbol{\omega}}_k\times]^2 \tag{22b}$$

$$k = 0, 1, \ldots$$

Substituting Eq. (22) into Eq. (21) gives

$$\begin{aligned}\Phi_{11_k} &= I_3 + \sum_{k=0}^{\infty} \frac{\Delta t^{2k+2} \left[\hat{\boldsymbol{\omega}}_k \times\right]^{2k+2}}{(2k+2)!} - \sum_{k=0}^{\infty} \frac{\Delta t^{2k+1} \left[\hat{\boldsymbol{\omega}}_k \times\right]^{2k+1}}{(2k+1)!} \\ &= I_3 + \sum_{k=0}^{\infty} \frac{(-1)^k \Delta t^{2k+2} \|\hat{\boldsymbol{\omega}}_k\|^{2k} \left[\hat{\boldsymbol{\omega}}_k \times\right]^2}{(2k+2)!} - \sum_{k=0}^{\infty} \frac{(-1)^k \Delta t^{2k+1} \|\hat{\boldsymbol{\omega}}_k\|^{2k} \left[\hat{\boldsymbol{\omega}}_k \times\right]}{(2k+1)!} \\ &= I_3 + \frac{\left[\hat{\boldsymbol{\omega}}_k \times\right]^2}{\|\hat{\boldsymbol{\omega}}_k\|^2} \sum_{k=0}^{\infty} \frac{(-1)^k \left(\|\hat{\boldsymbol{\omega}}_k\| \Delta t\right)^{2k+2}}{(2k+2)!} - \frac{\left[\hat{\boldsymbol{\omega}}_k \times\right]}{\|\hat{\boldsymbol{\omega}}_k\|} \sum_{k=0}^{\infty} \frac{(-1)^k \left(\|\hat{\boldsymbol{\omega}}_k\| \Delta t\right)^{2k+1}}{(2k+1)!}\end{aligned} \tag{23}$$

Power series expansions for sine and cosine are given by

$$\sin(x) = \sum_{j=0}^{\infty} \frac{(-1)^j x^{2j+1}}{(2j+1)!} \tag{24a}$$

$$\cos(x) = \sum_{j=0}^{\infty} \frac{(-1)^j x^{2j}}{(2j)!} \tag{24b}$$

Using these expansions, the submatrix Φ_{11_k} can be simplified to

$$\Phi_{11_k} = I_3 + \frac{\left[\hat{\boldsymbol{\omega}}_k \times\right]^2}{\|\hat{\boldsymbol{\omega}}_k\|^2} \left\{1 - \cos\left(\|\hat{\boldsymbol{\omega}}_k\| \Delta t\right)\right\} - \frac{\left[\hat{\boldsymbol{\omega}}_k \times\right]}{\|\hat{\boldsymbol{\omega}}_k\|} \sin\left(\|\hat{\boldsymbol{\omega}}_k\| \Delta t\right) \tag{25}$$

Using the same approach, both Φ_{12_k} and Φ_{13_k} can be calculated by

$$\Phi_{12_k} = \Delta t I_3 + \frac{\left[\hat{\boldsymbol{\omega}}_k \times\right]^2}{\|\hat{\boldsymbol{\omega}}_k\|^3} \left\{\|\hat{\boldsymbol{\omega}}_k\| \Delta t - \sin\left(\|\hat{\boldsymbol{\omega}}_k\| \Delta t\right)\right\} - \frac{\left[\hat{\boldsymbol{\omega}}_k \times\right]}{\|\hat{\boldsymbol{\omega}}_k\|^2} \left\{1 - \cos\left(\|\hat{\boldsymbol{\omega}}_k\| \Delta t\right)\right\} \tag{26a}$$

$$\begin{aligned}\Phi_{13_k} = -\Bigg(&\frac{\Delta t^2}{4} I_3 + \frac{\left[\hat{\boldsymbol{\omega}}_k \times\right]^2}{2\|\hat{\boldsymbol{\omega}}_k\|^4} \left\{-1 + \frac{\|\hat{\boldsymbol{\omega}}_k\|^2 \Delta t^2}{2} + \cos\left(\|\hat{\boldsymbol{\omega}}_k\| \Delta t\right)\right\} \\ &- \frac{\left[\hat{\boldsymbol{\omega}}_k \times\right]}{2\|\hat{\boldsymbol{\omega}}_k\|^3} \left\{\|\hat{\boldsymbol{\omega}}_k\| \Delta t - \sin\left(\|\hat{\boldsymbol{\omega}}_k\| \Delta t\right)\right\}\Bigg) \Gamma\end{aligned} \tag{26b}$$

The conversion from the spectral density $Q(t)$ to discrete-time covariance Q_k is given by

$$Q_k = \int_0^{\Delta t} \Phi(t) G(t) Q(t) G^T(t) \Phi^T(t) \, dt \tag{27}$$

Substituting Eq. (20) into Eq. (27) yields

$$\begin{aligned} W(t) &\equiv \Phi(t) G(t) Q(t) G^T(t) \Phi^T(t) \\ &= \begin{bmatrix} \frac{1}{4}\sigma_v^2 \Phi_{12} \Gamma\Gamma^T \Phi_{12}^T + \sigma_u^2 \Phi_{13} \Phi_{13}^T & \frac{1}{4}\sigma_v^2 \Phi_{12} \Gamma\Gamma^T - \frac{1}{2}\sigma_u^2 t \Phi_{13} \Gamma^T & \sigma_u^2 \Phi_{13} \\ \frac{1}{4}\sigma_v^2 \Gamma\Gamma^T \Phi_{12}^T - \frac{1}{2}\sigma_u^2 t \Gamma \Phi_{13}^T & \frac{1}{4}\sigma_v^2 \Gamma\Gamma^T + \frac{1}{4}\sigma_v^2 t^2 \Gamma\Gamma^T & -\frac{1}{2}\sigma_u^2 t \Gamma \\ \sigma_u^2 \Phi_{13}^T & -\frac{1}{2}\sigma_u^2 t \Gamma^T & \sigma_u^2 I_{3n} \end{bmatrix} \end{aligned} \tag{28}$$

The lower right blocks can be directly calculated by

$$\begin{aligned} Q_{22_k} &= \int_0^{\Delta t} \frac{1}{4}\sigma_v^2 \Gamma\Gamma^T + \frac{1}{4}\sigma_u^2 t^2 \Gamma\Gamma^T dt \\ &= \left(\frac{1}{4}\sigma_v^2 \Delta t + \frac{1}{12}\sigma_u^3 \Delta t^3 \right) \Gamma\Gamma^T \end{aligned} \tag{29a}$$

$$Q_{23_k} = Q_{23_k}^T = \int_0^{\Delta t} -\frac{1}{2}\sigma_u^2 t dt = -\frac{1}{4}\sigma_u^2 \Delta t^2 \Gamma \tag{29b}$$

$$Q_{33_k} = \int_0^{\Delta t} \sigma_u^2 dt I_{3n} = \sigma_u^2 \Delta t I_{3n} \tag{29c}$$

Assuming that the sampling rate is below Nyquist's limit,[16] the calculation of other blocks in Q_k can be approximated by

$$\begin{aligned} Q_{11_k} &= \int_0^{\Delta t} \frac{1}{4}\sigma_v^2 \Phi_{12} \Gamma\Gamma^T \Phi_{12}^T + \sigma_u^2 \Phi_{13} \Phi_{13}^T dt \\ &\approx \int_0^{\Delta t} \left(\frac{1}{4}\sigma_v^2 t^2 + \frac{1}{16}\sigma_u^2 t^4 \right) dt \, \Gamma\Gamma^T \\ &= \left(\frac{1}{12}\sigma_v^2 \Delta t^3 + \frac{1}{80}\sigma_u^2 \Delta t^5 \right) \Gamma\Gamma^T \end{aligned} \tag{30a}$$

$$\begin{aligned} Q_{12_k} = Q_{21_k}^T &= \int_0^{\Delta t} \frac{1}{4}\sigma_v^2 \Phi_{12} \Gamma\Gamma^T - \frac{1}{2}\sigma_u^2 t \Phi_{13} \Gamma^T dt \\ &\approx \int_0^{\Delta t} \left(\frac{1}{4}\sigma_v^2 t + \frac{1}{8}\sigma_u^2 t^3 \right) dt \, \Gamma\Gamma^T \\ &= \left(\frac{1}{8}\sigma_v^2 \Delta t^2 + \frac{1}{32}\sigma_u^2 \Delta t^4 \right) \Gamma\Gamma^T \end{aligned} \tag{30b}$$

$$\begin{aligned} Q_{13_k} = Q_{31_k}^T &= \int_0^{\Delta t} \sigma_u^2 \Phi_{13} dt \\ &\approx -\int_0^{\Delta t} \frac{1}{4}\sigma_u^2 t^2 dt \, \Gamma = -\frac{1}{12}\sigma_u^2 \Delta t^3 \Gamma \end{aligned} \tag{30c}$$

Finally, the discrete-time attitude kinematics model is given by[16]

$$\boldsymbol{q}_{k+1} = \Theta(\boldsymbol{\omega}_k) \boldsymbol{q}_k \tag{31}$$

where the matrix $\Theta(\boldsymbol{\omega}_k)$ can also be derived using a power series approach, which is given by

$$\Theta(\boldsymbol{\omega}_k) = \begin{bmatrix} \cos\left(\frac{1}{2}\|\boldsymbol{\omega}_k\|\Delta t\right) I_3 - [\boldsymbol{\Psi}_k \times] & \boldsymbol{\Psi}_k \\ -\boldsymbol{\Psi}_k^T & \cos\left(\frac{1}{2}\|\boldsymbol{\omega}_k\|\Delta t\right) \end{bmatrix} \tag{32a}$$

$$\boldsymbol{\Psi}_k \equiv \frac{\sin\left(\frac{1}{2}\|\boldsymbol{\omega}_k\|\Delta t\right)}{\|\boldsymbol{\omega}_k\|}\boldsymbol{\omega}_k \tag{32b}$$

B. Extended Kalman Filter

A multiplicative EKF is used here as the estimator.[18] The filter proceeds in two steps: propagation and measurement update. The propagation step propagates the estimated states to the next observation time, while the measurement update step updates the propagated states based on the measurements from the sensors. Details of the multiplicative EKF estimator are shown in Figure 3.

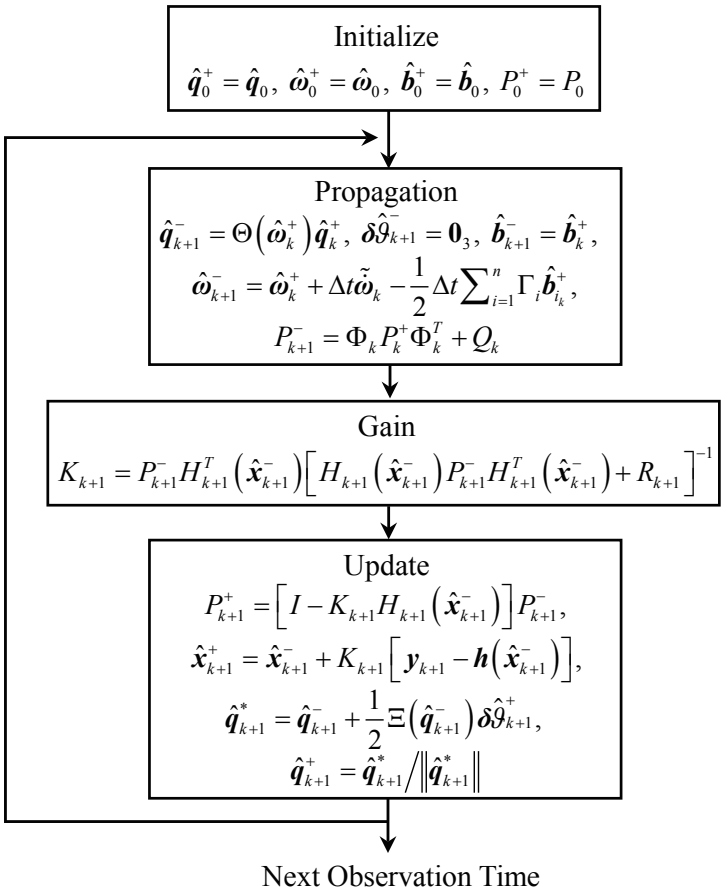

Figure 3. Flowchart of Multiplicative EKF Estimator

C. Parameter Specifications

In this section, the parameters for the following simulations of a Mars approach scenario are specified. Assuming that no control force is exerted, the control acceleration at the mass center $\boldsymbol{u}_c$ equals to zero. Furthermore, to simulate a change in rotational motion of the vehicle, the control torques are assumed to be zero so that $\boldsymbol{M} = [0, 0, 0]^T$. The propagation of the true angular velocity is governed by

$$\dot{\boldsymbol{\omega}} = \boldsymbol{M} - J^{-1}\left[\boldsymbol{\omega} \times (J\boldsymbol{\omega})\right] \tag{33}$$

where $J = \text{diag}\,(J_x, J_y, J_z)$ is the moment of inertia of the vehicle. Therefore, given the initial quaternion and angular velocity, set to $\boldsymbol{q}_0 = [0, 0, 0, 1]^T$ and $\boldsymbol{\omega}_0 = [0.1, 0, 0.01]^T$ deg/s, respectively, the true quaternion, angular velocity, and angular acceleration can be generated.

The attitude determination system, shown in Figure 2, consists of a star tracker and three-axis gyro sensor suite. A multiplicative EKF is used to estimate the attitude and gyro biases.[21] The star tracker is simulated to generate the vector observations as well as their associated measurement noise. The optical axis of the star tracker is assumed to be aligned with the z axis of the body frame. The sensor field of view is 6 degrees, and the sensor precision is 0.005 degrees (3σ). The maximum number of allowable measurement stars at each time is 10. The spectral densities for the three-axis gyro are given by $\sigma_{gu}^2 I_3$ and $\sigma_{gv}^2 I_3$ respectively. In the following simulations, the values of σ_{gu} and σ_{gv} are set to $\sqrt{10} \times 10^{-10}$ rad/s$^{3/2}$ and $\sqrt{10} \times 10^{-7}$ rad/s$^{1/2}$, respectively. More details on the attitude determination can be found in Ref. 16. The other parameters for the simulation are summarized in Table 1. The time duration of one simulation run is 200 seconds. The true biases of the accelerometers, quaternions, angular velocity, and the number of available stars are illustrated in Figure 4.

Table 1. Parameters for the Simulation

Parameter	Value	Unit
J_x	261	kg-m^2
J_y	294	kg-m^2
J_z	212	kg-m^2
$\boldsymbol{b}_1$	$[-3 \times 10^{-4}, 2.5 \times 10^{-4}, 1 \times 10^{-4}]^T$	m/s^2
$\boldsymbol{b}_2$	$[2 \times 10^{-4}, -1.5 \times 10^{-4}, -2 \times 10^{-4}]^T$	m/s^2
$\boldsymbol{b}_3$	$[-1 \times 10^{-4}, 3 \times 10^{-4}, -2.5 \times 10^{-4}]^T$	m/s^2
σ_u	1×10^{-6}	m/s$^{5/2}$
σ_v	1×10^{-5}	m/s$^{3/2}$
Δt	1	s

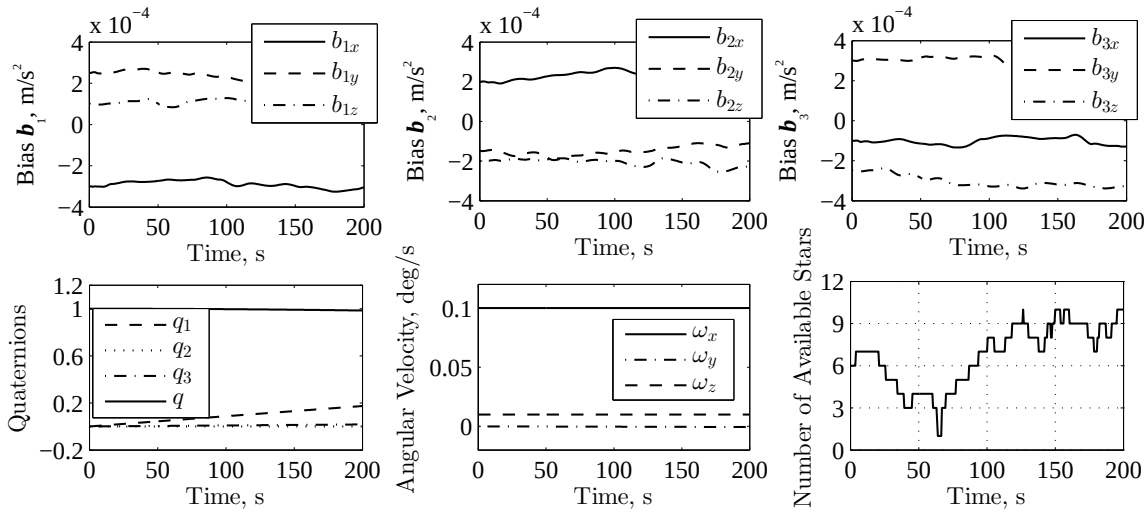

Figure 4. True Biases, Quaternions, Angular Velocity, and the Number of Available Stars

D. Observability Analysis

For the observability analysis three accelerometers are calibrated using the EKF without modification. The parameters from Table 1 are used. The simulation is run 500 times, and the estimation errors and 3σ error bounds for the attitude and angular velocity are shown in Figure 5, while the calibration errors and 3σ bounds of the biases from four randomly selected simulations are shown in Figure 6.

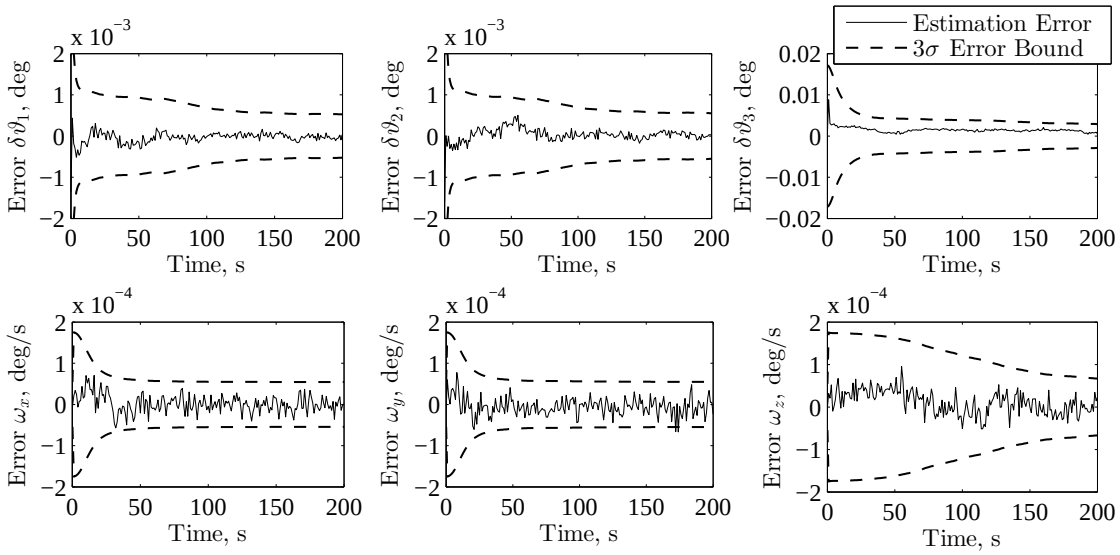

Figure 5. Attitude and Angular Velocity Errors Based Solely on the EKF

The simulation results show that both the attitude and angular velocity can be accurately estimated from the EKF, and the estimation errors are well bounded. Comparing with Figure

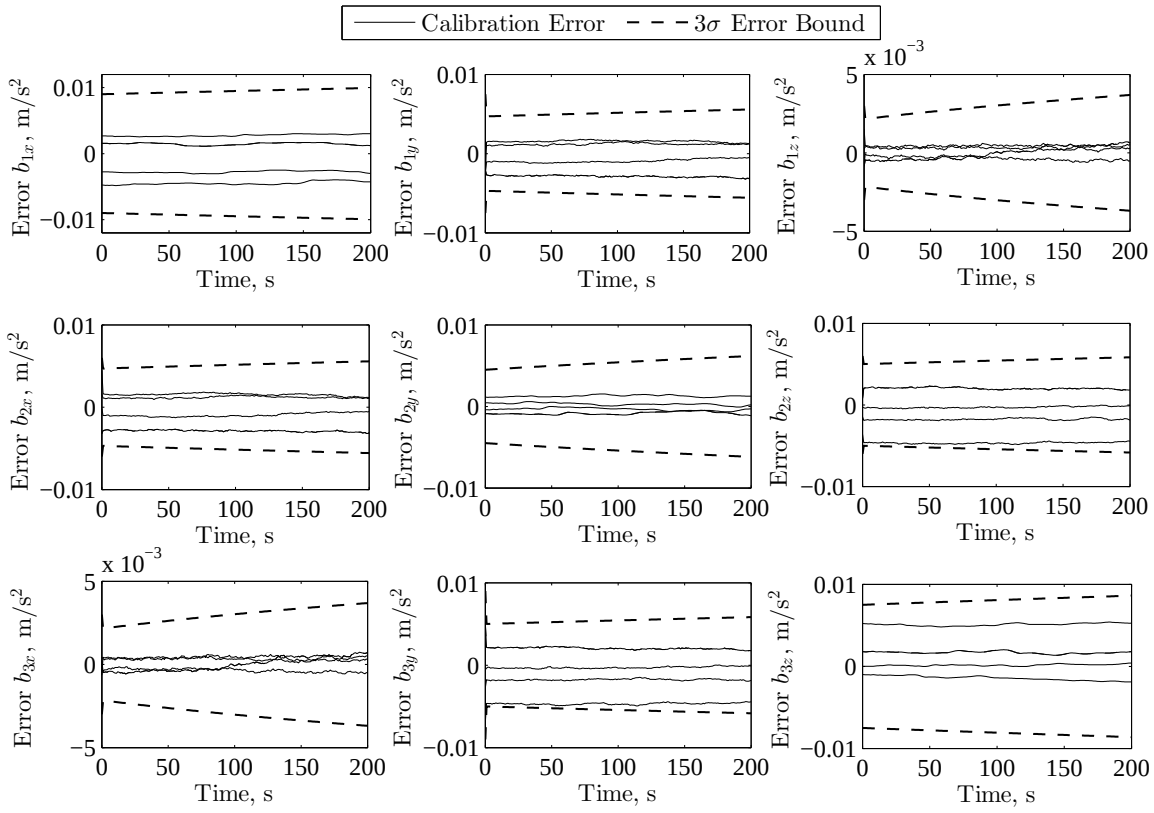

Figure 6. Calibration Errors Based Solely on the EKF

4, it is also found that the number of available stars is the main contributor to the attitude estimation performance. That is, more vector observations from the star tracker generally leads to more accurate attitude estimates. However, the estimation errors of both $\boldsymbol{\delta\vartheta}$ and $\boldsymbol{\omega}$ in the z axis are larger than those in the x and y axes. This is due to the fact that the optical axis of the star tracker is aligned with the z axis of the body frame, and the sensor field of view is narrow. This will ultimately influence the performance of the accelerometer calibration system because the attitude and angular velocity from the attitude determination system are used as observations. From Figure 6 it is clear that the simulation results also demonstrate poor estimation of the accelerometer biases. The errors in the biases are mostly based on the initial values, and the 3σ bounds diverge with time. Therefore, the accelerometer biases cannot be determined based solely on the EKF. This situation can be explained by the following observability analysis.

Based on the discrete-time model, a first-order approximation of the state transition matrix is used here to simplify the derivation while reflecting the feature of the calibration

system:

$$\Phi_k \approx \begin{bmatrix} I_3 - \Delta t\,[\hat{\boldsymbol{\omega}}_k\times] & \Delta t I_3 & O_{3\times 3n} \\ O_{3\times 3} & I_3 & -\frac{1}{2}\Delta t\Gamma \\ O_{3n\times 3} & O_{3n\times 3} & I_{3n} \end{bmatrix} \equiv \begin{bmatrix} \Lambda_k & \Delta t I_3 & O_{3\times 3n} \\ O_{3\times 3} & I_3 & -\frac{1}{2}\Delta t\Gamma \\ O_{3n\times 3} & O_{3n\times 3} & I_{3n} \end{bmatrix} \tag{34}$$

Powers of Φ_k can be calculated by

$$\Phi_k^j = \begin{bmatrix} \Lambda_k^j & \Delta t\sum_{i=1}^{j}\Lambda_k^{i-1} & -\frac{1}{2}\Delta t^2\sum_{i=1}^{j-1}(j-i)\,\Lambda_k^{i-1}\Gamma \\ O_{3\times 3} & I_3 & -\frac{j}{2}\Delta t\Gamma \\ O_{3n\times 3} & O_{3n\times 3} & I_{3n} \end{bmatrix},\ j>1 \tag{35}$$

where $\Lambda_k^0 = I_3$. Because the dimension of the state vector is $3n+6$, the observability matrix is given by

$$O_k = \begin{bmatrix} H_k \\ \vdots \\ H_k\Phi_k^{3n+5} \end{bmatrix} \tag{36}$$

where

$$\begin{aligned} H_k\Phi_k^j &= \begin{bmatrix} \Lambda_k^j & \Delta t\sum_{i=1}^{j}\Lambda_k^{i-1} & -\frac{1}{2}\Delta t^2\sum_{i=1}^{j-1}(j-i)\,\Lambda_k^{i-1}\Gamma \\ O_{3\times 3} & I_3 & -\frac{j}{2}\Delta t\Gamma \end{bmatrix} \\ &\equiv \left[\Upsilon_{\boldsymbol{\delta\vartheta}}^j, \Upsilon_{\boldsymbol{\omega}}^j, \Upsilon_{\boldsymbol{b}}^j\right] \end{aligned} \tag{37}$$

The left, middle, and right blocks of this matrix indicate the relationship between the observations and the states of $\boldsymbol{\delta\vartheta}$, $\boldsymbol{\omega}$, and $\boldsymbol{b}$ respectively, which can be used for the observability analysis. It is evident that the rank of $\Upsilon_{\boldsymbol{\delta\vartheta}}^j$ and $\Upsilon_{\boldsymbol{\omega}}^j$ equals to three which means that $\boldsymbol{\delta\vartheta}$ and $\boldsymbol{\omega}$ are observable. Furthermore, because the matrix $\Upsilon_{\boldsymbol{b}}^j$ is constructed by the linear combinations of Γ, the rank of the $\Upsilon_{\boldsymbol{b}}^j$ is equal to the rank of Γ. Because the dimension of $\boldsymbol{b}_k$ is $3n$, while the dimension of Γ is three at most, the accelerometer biases are not observable. This explains why the estimation errors in the biases do not converge. However, it is evident that a linear combination $\Gamma\boldsymbol{b}_k$ of these biases is observable.

In order to demonstrate the analytical result, consider the simplest case: three accelerometers mounted at positions

$$\boldsymbol{r}_1 = \begin{bmatrix} 1 \\ 0 \\ 0 \end{bmatrix}, \quad \boldsymbol{r}_2 = \begin{bmatrix} 0 \\ 1 \\ 0 \end{bmatrix}, \quad \boldsymbol{r}_3 = \begin{bmatrix} 0 \\ 0 \\ 1 \end{bmatrix} \tag{38}$$

such that the position matrix R is the identity matrix. Without loss in generality it is

assumed that the reference frame of each accelerometer is identical to the body frame, so that $T_i^b = I_3$. Therefore, Γ is given by

$$\Gamma = \begin{bmatrix} 0 & 0 & 0 & 0 & 0 & -1 & 0 & 1 & 0 \\ 0 & 0 & 1 & 0 & 0 & 0 & -1 & 0 & 0 \\ 0 & -1 & 0 & 1 & 0 & 0 & 0 & 0 & 0 \end{bmatrix} \tag{39}$$

The observable linear combination of the biases is

$$\Gamma \boldsymbol{b}_k = \left. \begin{bmatrix} b_{3y} - b_{2z} \\ b_{1z} - b_{3x} \\ b_{2x} - b_{1y} \end{bmatrix} \right|_{t_k} \tag{40}$$

Equation (40) is now used to calculate the linear combination of the estimated biases from the full filter, which provides estimates for all the (unobservable) biases. The relationship between each estimated and true accelerometer bias is given by

$$\hat{b}_{ix} = b_{ix} + \epsilon_{ix}, \quad i = 1,\, 2,\, 3 \tag{41a}$$

$$\hat{b}_{iy} = b_{iy} + \epsilon_{iy}, \quad i = 1,\, 2,\, 3 \tag{41b}$$

$$\hat{b}_{iz} = b_{iz} + \epsilon_{iz}, \quad i = 1,\, 2,\, 3 \tag{41c}$$

where $\hat{b}_{ix}$, $\hat{b}_{iy}$ and $\hat{b}_{iz}$ are estimated biases, and ϵ_{ix}, ϵ_{iy} and ϵ_{iz} are their respective estimation errors. The symmetrical covariance matrix $P_{\Gamma \boldsymbol{b}}$ of $\Gamma \boldsymbol{b}_k$ can be calculated by

$$P_{\Gamma \boldsymbol{b}_{11}} = E\left\{(\epsilon_{3y} - \epsilon_{2z})^2\right\} = E\left\{\epsilon_{3y}^2\right\} - 2E\left\{\epsilon_{3y}\epsilon_{2z}\right\} + E\left\{\epsilon_{2z}^2\right\} \tag{42a}$$

$$\begin{aligned} P_{\Gamma \boldsymbol{b}_{12}} &= P_{\Gamma \boldsymbol{b}_{21}} = E\left\{(\epsilon_{3y} - \epsilon_{2z})\,(\epsilon_{1z} - \epsilon_{3x})\right\} \\ &= E\left\{\epsilon_{3y}\epsilon_{1z}\right\} - E\left\{\epsilon_{2z}\epsilon_{1z}\right\} - E\left\{\epsilon_{3y}\epsilon_{3x}\right\} + E\left\{\epsilon_{2z}\epsilon_{3x}\right\} \end{aligned} \tag{42b}$$

$$\begin{aligned} P_{\Gamma \boldsymbol{b}_{13}} &= P_{\Gamma \boldsymbol{b}_{31}} = E\left\{(\epsilon_{3y} - \epsilon_{2z})\,(\epsilon_{2x} - \epsilon_{1y})\right\} \\ &= E\left\{\epsilon_{3y}\epsilon_{2x}\right\} - E\left\{\epsilon_{2z}\epsilon_{2x}\right\} - E\left\{\epsilon_{3y}\epsilon_{1y}\right\} + E\left\{\epsilon_{2z}\epsilon_{1y}\right\} \end{aligned} \tag{42c}$$

$$P_{\Gamma \boldsymbol{b}_{22}} = E\left\{(\epsilon_{1z} - \epsilon_{3x})^2\right\} = E\left\{\epsilon_{1z}^2\right\} - 2E\left\{\epsilon_{1z}\epsilon_{3x}\right\} + E\left\{\epsilon_{3x}^2\right\} \tag{42d}$$

$$\begin{aligned} P_{\Gamma \boldsymbol{b}_{23}} &= P_{\Gamma \boldsymbol{b}_{32}} = E\left\{(\epsilon_{1z} - \epsilon_{3x})\,(\epsilon_{2x} - \epsilon_{1y})\right\} \\ &= E\left\{\epsilon_{1z}\epsilon_{2x}\right\} - E\left\{\epsilon_{3x}\epsilon_{2x}\right\} - E\left\{\epsilon_{1z}\epsilon_{1y}\right\} + E\left\{\epsilon_{3x}\epsilon_{1y}\right\} \end{aligned} \tag{42e}$$

$$P_{\Gamma \boldsymbol{b}_{33}} = E\left\{(\epsilon_{2x} - \epsilon_{1y})^2\right\} = E\left\{\epsilon_{2x}^2\right\} - 2E\left\{\epsilon_{2x}\epsilon_{1y}\right\} + E\left\{\epsilon_{1y}^2\right\} \tag{42f}$$

Therefore, the covariance matrix $P_{\Gamma \boldsymbol{b}}$ can be simply calculated by the elements of the covariance matrix P_k from the filter, i.e. all the expectations in Eq. (42) are given from the

elements of P_k. The estimation errors and 3σ error bounds of the linear combination of the biases are shown in Figure 7.

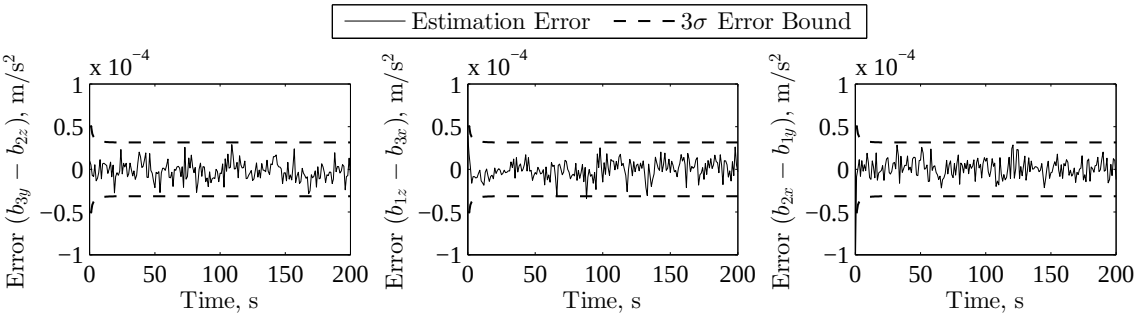

Figure 7. Estimation Errors of the Linear Combination of the Biases

The simulation results also prove that the linear combination of the biases can be accurately estimated. Furthermore, according to Eq. (9) the matrix Γ is given by

$$\Gamma = -2\frac{\partial \dot{\boldsymbol{\omega}}}{\partial \boldsymbol{b}^T} \tag{43}$$

This indicates that an accurate estimate of the linear combination of the biases may lead to accurate angular acceleration estimation. To demonstrate the improved accuracy in the angular acceleration estimation process, a comparative scenario in which the angular acceleration is computed directly from the accelerometer outputs is considered. The estimation errors of the angular acceleration estimates from the two methods are generated and illustrated in Figure 8. Here, the filtering method denotes the linear combination estimates derived from Eq. (40) using the estimated biases, while the direct method denotes using Eq. (9), which includes the unfiltered biases.

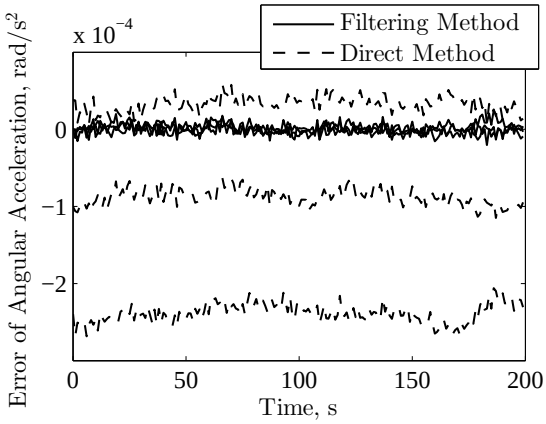

Figure 8. Angular Acceleration Estimate Errors Using the Filtering Method and Direct Method

It is concluded that the filtering approach indeed improves the estimation accuracy for the angular acceleration. Because no information on the accelerometer biases is provided in the direct method, the angular acceleration is poorly estimated due to the unknown biases. Note that this is also true for the full filter that produced the bias estimates represented by Figure 6 because they are poorly estimated. Furthermore, the estimation result for the direct method is very sensitive to the measurement noise in the accelerometers. However, based on the previous analysis, although not all biases can be determined in the filtering approach, accurately estimating a linear combination of the biases improves the accuracy and stability of the angular acceleration estimates. Based on this discovery, a recalculation process after the filtering approach is introduced using these more accurate angular acceleration estimates to further eliminate the estimation errors from the accelerometer biases.

E. Recalculation Process

In the recalculation process, the biases for the accelerometers are computed by the updated biases and angular velocity from the estimator. First, based on Eq. (9), the angular acceleration is estimated by

$$\hat{\dot{\boldsymbol{\omega}}}_k = \tilde{\dot{\boldsymbol{\omega}}}_k - \frac{1}{2}\sum_{i=1}^{n} \Gamma_i \hat{\boldsymbol{b}}_{i_k}^{+} \tag{44}$$

Then together with the updated angular velocity, the matrix $\bar{\Omega}_k$ can be estimated by

$$\hat{\bar{\Omega}}_k = \Omega_k^2\left(\hat{\boldsymbol{\omega}}_k^{+}\right) + \dot{\Omega}_k\left(\hat{\dot{\boldsymbol{\omega}}}_k\right) \tag{45}$$

According to Eqs. (2) and (3), the accelerometer biases are recalculated using

$$\hat{\boldsymbol{b}}_{i_k}^{++} = \tilde{\boldsymbol{f}}_{i_k} - \left(T_i^b\right)^T\left(\boldsymbol{u}_{c_k} + \hat{\bar{\Omega}}_k \boldsymbol{r}_i\right) \tag{46}$$

Discrete-time equations are required for $\tilde{\boldsymbol{f}}_{i_k}$ and $\hat{\bar{\Omega}}_k$. Substituting Eq. (5b) into Eq. (5a) and using one time-step back leads to

$$\tilde{\boldsymbol{f}}_{i_k} = \boldsymbol{f}_{i_k} + \boldsymbol{b}_{i_k} + \boldsymbol{\eta}_{uvi_k} \tag{47}$$

where

$$\boldsymbol{\eta}_{uvi_k} \equiv \left(\frac{\sigma_v^2}{\Delta t} + \frac{1}{12}\sigma_u^2\,\Delta t\right)^{1/2}\mathbf{N}_{vi_k} - \frac{1}{2}\sigma_u\,\Delta t^{1/2}\mathbf{N}_{ui_k} \tag{48}$$

Note that $\mathbf{N}_{ui_k}$ and $\mathbf{N}_{vi_k}$ are supposed to be evaluated at time t_{k-1}, but because they are white-noise processes they can be written at time t_k. Using the same approach to derive

Eq. (47), the discrete version of Eq. (9) is given by

$$\dot{\boldsymbol{\omega}}_k = \tilde{\dot{\boldsymbol{\omega}}}_k - \frac{1}{2}\Gamma \boldsymbol{b}_k - \frac{1}{2}\sum_{i=1}^{n} \Gamma_i \boldsymbol{\eta}_{uvi_k} \tag{49}$$

Substituting Eq. (47) and Eq. (49) into Eq. (46) yields

$$\begin{aligned}
\hat{\boldsymbol{b}}_{i_k}^{++} &= \boldsymbol{f}_{i_k} + \boldsymbol{b}_{i_k} + \boldsymbol{\eta}_{uvi_k} - \left(T_i^b\right)^T \boldsymbol{u}_{c_k} \\
&\quad - \left(T_i^b\right)^T \left(\Omega_k^2 \left(\hat{\boldsymbol{\omega}}_k^+\right) + \left[\left(\dot{\boldsymbol{\omega}}_k + \frac{1}{2}\Gamma \boldsymbol{b}_k + \frac{1}{2}\sum_{i=1}^{n} \Gamma_i \boldsymbol{\eta}_{uvi_k} - \frac{1}{2}\Gamma \hat{\boldsymbol{b}}_k^+ \right) \times \right] \right) \boldsymbol{r}_i \\
&= \boldsymbol{f}_{i_k} + \boldsymbol{b}_{i_k} - \left(T_i^b\right)^T \boldsymbol{u}_{c_k} + \left(T_i^b\right)^T [\boldsymbol{r}_i \times] \left(\dot{\boldsymbol{\omega}}_k + \frac{1}{2}\Gamma \boldsymbol{b}_k \right) \\
&\quad - \left(T_i^b\right)^T \Omega_k^2 \left(\hat{\boldsymbol{\omega}}_k^+\right) \boldsymbol{r}_i - \frac{1}{2}\left(T_i^b\right)^T [\boldsymbol{r}_i \times] \Gamma \hat{\boldsymbol{b}}_k^+ \\
&\quad + \boldsymbol{\eta}_{uvi_k} + \frac{1}{2}\left(T_i^b\right)^T [\boldsymbol{r}_i \times] \Gamma \boldsymbol{\eta}_{uv_k}
\end{aligned} \tag{50}$$

where $\boldsymbol{\eta}_{uv_k} = \left[\boldsymbol{\eta}_{uv1_k}^T, \ldots, \boldsymbol{\eta}_{uvn_k}^T\right]^T$. Several noise terms appear in Eq. (50). To derive its covariance, possible correlations between noise terms should be investigated. Equation (50) is abbreviated as

$$\hat{\boldsymbol{b}}_{i_k}^{++} = \boldsymbol{b}\left(\tilde{\boldsymbol{f}}_k, \hat{\boldsymbol{\omega}}_k^+, \hat{\boldsymbol{b}}_k^+\right) \tag{51}$$

It is evident from the EKF that the output of the accelerometers are only used to propagate the model used for the accelerometer calibration process, not to update the states. Therefore, accelerometer outputs are related to the propagated angular velocity. The propagation and update equations for angular velocity can be modeled by

$$\hat{\boldsymbol{\omega}}_k^- = \boldsymbol{\omega}^-\left(\hat{\boldsymbol{\omega}}_{k-1}^+, \hat{\boldsymbol{b}}_{k-1}^+, \tilde{\boldsymbol{f}}_{k-1}\right) \tag{52a}$$

$$\hat{\boldsymbol{\omega}}_k^+ = \boldsymbol{\omega}^+\left(\boldsymbol{\delta}\hat{\boldsymbol{\vartheta}}_k^-, \hat{\boldsymbol{\omega}}_k^-, \hat{\boldsymbol{b}}_k^-, \boldsymbol{y}_k\right) \tag{52b}$$

This indicates that in Eq. (50) $\hat{\boldsymbol{\omega}}_k^+$ is only related to $\tilde{\boldsymbol{f}}_{k-1}$, not to $\tilde{\boldsymbol{f}}_k$, so $\hat{\boldsymbol{\omega}}_k^+$ and $\tilde{\boldsymbol{f}}_k$ are uncorrelated. Furthermore, no correlation exists between $\hat{\boldsymbol{b}}_k^+$ and $\tilde{\boldsymbol{f}}_k$ either.

Here only the biases of the accelerometers are recalculated, and the attitude error and

angular velocity remain the same, so the sensitivity matrix can be defined by

$$\begin{aligned} H_k^b &= \frac{\partial \hat{\boldsymbol{x}}_k^{++}}{\partial \left(\hat{\boldsymbol{x}}_k^{+}\right)^T} \\ &= \begin{bmatrix} I_3 & O_{3\times 3} & O_{3\times 3n} \\ O_{3\times 3} & I_3 & O_{3\times 3n} \\ O_{3n\times 3} & S_\omega & S_b \end{bmatrix} \end{aligned} \tag{53}$$

where

$$S_\omega = \begin{bmatrix} -\left(T_i^b\right)^T \left(r_{1x}\Omega_1^\omega + r_{1y}\Omega_2^\omega + r_{1z}\Omega_3^\omega\right) \\ \vdots \\ -\left(T_n^b\right)^T \left(r_{nx}\Omega_1^\omega + r_{ny}\Omega_2^\omega + r_{nz}\Omega_3^\omega\right) \end{bmatrix} \tag{54a}$$

$$S_b = -\frac{1}{2}\begin{bmatrix} \left(T_1^b\right)^T \left[\boldsymbol{r}_1\times\right]\Gamma \\ \vdots \\ \left(T_n^b\right)^T \left[\boldsymbol{r}_n\times\right]\Gamma \end{bmatrix} \tag{54b}$$

In this equation, $\boldsymbol{r}_i = [r_{ix}, r_{iy}, r_{iz}]^T$, and

$$\Omega_1^\omega = \begin{bmatrix} 0 & -2\hat{\omega}_{y_k}^+ & -2\hat{\omega}_{z_k}^+ \\ \hat{\omega}_{y_k}^+ & \hat{\omega}_{x_k}^+ & 0 \\ \hat{\omega}_{z_k}^+ & 0 & \hat{\omega}_{x_k}^+ \end{bmatrix} \tag{55a}$$

$$\Omega_2^\omega = \begin{bmatrix} \hat{\omega}_{y_k}^+ & \hat{\omega}_{x_k}^+ & 0 \\ -2\hat{\omega}_{x_k}^+ & 0 & -2\hat{\omega}_{z_k}^+ \\ 0 & \hat{\omega}_{z_k}^+ & \hat{\omega}_{y_k}^+ \end{bmatrix} \tag{55b}$$

$$\Omega_3^\omega = \begin{bmatrix} \hat{\omega}_{z_k}^+ & 0 & \hat{\omega}_{x_k}^+ \\ 0 & \hat{\omega}_{z_k}^+ & \hat{\omega}_{y_k}^+ \\ -2\hat{\omega}_{x_k}^+ & -2\hat{\omega}_{y_k}^+ & 0 \end{bmatrix} \tag{55c}$$

By defining the matrix

$$M = \frac{1}{2}\begin{bmatrix} \left(T_1^b\right)^T \left[\boldsymbol{r}_1\times\right]\Gamma \\ \vdots \\ \left(T_n^b\right)^T \left[\boldsymbol{r}_n\times\right]\Gamma \end{bmatrix} + I_{3n} \tag{56}$$

the covariance matrix for the associated noise processes in Eq. (50) is defined by Q_k^b, which

is a $(3n+6)\times(3n+6)$ square matrix:

$$Q_k^b = \begin{bmatrix} O_{6\times 6} & O_{6\times 3n} \\ O_{3n\times 6} & \sigma_{uv}^2 M M^T \end{bmatrix} \tag{57}$$

where $\sigma_{uv}^2 \equiv \frac{\sigma_v^2}{\Delta t} + \frac{1}{3}\sigma_u^2 \Delta t$. The recalculation of the covariance is thus given by

$$P_k^{++} = H_k^b P_k^+ \left(H_k^b\right)^T + Q_k^b \tag{58}$$

After the recalculation process, both $\hat{\boldsymbol{b}}_k^+$ and P_k^+ are replaced with $\hat{\boldsymbol{b}}_k^{++} = \left[\boldsymbol{b}_1^{++T}, \ldots, \boldsymbol{b}_n^{++T}\right]^T$ and P_k^{++}, respectively, in the filter. Then the replaced biases are used to propagate the state to time t_{k+1}, and the replaced covariance is used to propagate the covariance to time t_{k+1} as well.

IV. Simulation Results

In this section, the Mars approach scenario is simulated to demonstrate the feasibility and performance of the proposed accelerometer calibration method. The same parameters are also taken from Table 1.

A. Optimality Analysis

As mentioned before, the EKF in the calibration system is not an optimal estimator due to the correlation problem. Actually, no matter what attitude information (the estimated attitude or the raw measurements) is provided to the calibration system, the correlation problem exists because the attitude is estimated in both systems. In order to determine a consistent estimate of the attitude, and to examine the optimality of the calibration system, a covariance intersection method[22] is introduced to estimate the attitude by fusing the estimation results from both the attitude determination and calibration systems.

Consider two estimated attitudes ($\boldsymbol{q}_k^1$, $\boldsymbol{q}_k^2$) and associated 3×3 covariance matrices ($P_{q_k}^1$, $P_{q_k}^2$) of the vector error-quaternion parts. Here the value of P_{q_k} can be calculated by the covariance matrix of the attitude errors through $P_{q_k} = \frac{1}{4}P_{\delta\vartheta_k}$. A consistent estimate of the fused covariance $P_{q_k}^f$ is given by

$$\left(P_{q_k}^f\right)^{-1} = w_1 \left(P_{q_k}^1\right)^{-1} + w_2 \left(P_{q_k}^2\right)^{-1} \tag{59}$$

where the weights w_1 and w_2 satisfy $w_1 + w_2 = 1$. Values of w_1 and w_2 can be found using a simple optimization scheme that minimizes the determinant of $P_{q_k}^f$. It has been proven that

minimizing the determinant of $P_{q_k}^f$ is a convex optimization problem, which indicates that the cost function has only one local optimum of weighting in the range of $[0, 1]$.[18] However, the traditional additive fusion of the quaternions cannot be used directly because the unit norm constraint of the resulting quaternion may not be guaranteed. Reference 23 derives a solution to this problem. In this reference, quaternion and non-attitude states are fused. Here, only the quaternions are fused because the angular velocity is estimated using two uncorrelated approaches in the decentralized estimation system shown in Figure 2. For this subproblem the fused quaternion $\boldsymbol{q}_k^f$ can be found by maximizing an appended objective function using the method of Lagrange multipliers:

$$J\left(\boldsymbol{q}_k^f\right) = -\sum_{i=1}^{2} w_i \left(\boldsymbol{q}_k^f\right)^T \Xi\left(\boldsymbol{q}_k^i\right) \left(P_{q_k}^i\right)^{-1} \Xi^T\left(\boldsymbol{q}_k^i\right) \boldsymbol{q}_k^f + \lambda\left[1 - \left(\boldsymbol{q}_k^f\right)^T \boldsymbol{q}_k^f\right] \tag{60}$$

where λ is the Lagrange multiplier. The necessary conditions for the maximization of J are

$$\frac{\partial J}{\partial \boldsymbol{q}_k^f} = -2\sum_{i=1}^{2} w_i\, \Xi\left(\boldsymbol{q}_k^i\right) \left(P_{q_k}^i\right)^{-1} \Xi^T\left(\boldsymbol{q}_k^i\right) \boldsymbol{q}_k^f - 2\lambda \boldsymbol{q}_k^f = \mathbf{0} \tag{61a}$$

$$\frac{\partial J}{\partial \lambda} = 1 - \left(\boldsymbol{q}_k^f\right)^T \boldsymbol{q}_k^f = 0 \tag{61b}$$

This leads to

$$\left(Z + \lambda I_4\right) \boldsymbol{q}_k^f = \mathbf{0} \tag{62}$$

where

$$Z = \sum_{i=1}^{2} w_i\, \Xi\left(\boldsymbol{q}_k^i\right) \left(P_{q_k}^i\right)^{-1} \Xi^T\left(\boldsymbol{q}_k^i\right) \tag{63}$$

Equation (62) represents an eigenvalue/eigenvector decomposition of the 4×4 matrix Z. The objective function in Eq. (60) can be rewritten as

$$J\left(\boldsymbol{q}_k^f\right) = -\left(\boldsymbol{q}_k^f\right)^T Z\, \boldsymbol{q}_k^f + \lambda\left[1 - \left(\boldsymbol{q}_k^f\right)^T \boldsymbol{q}_k^f\right] \tag{64}$$

From Eq. (62), $Z\boldsymbol{q}_k^f = -\lambda \boldsymbol{q}_k^f$. Substituting this expression into Eq. (64) leads to $J(\boldsymbol{q}_k^f) = \lambda$. The fused quaternion is thus given by finding the normalized eigenvector corresponding to the minimum eigenvalue of the matrix Z, because the eigenvalue is given by $-\lambda$ from $Z\boldsymbol{q}_k^f = -\lambda \boldsymbol{q}_k^f$. The sign of $\boldsymbol{q}_k^f$ can be determined based on the sign of $\boldsymbol{q}_k^1$ and $\boldsymbol{q}_k^2$.[23] The solution is equivalent to the matrix weighted average quaternion algorithm shown in Ref. 24.

On the other hand, the correlation problem can be overcome if the attitude is not estimated in the calibration system, and only the angular velocity is used as the observation. A comparative calibration scheme is thus considered. In this scheme the state, which only

includes the angular velocity and accelerometer biases, is also estimated using an EKF. The attitude is estimated by the attitude determination system. Meanwhile the observation is the angular velocity from the attitude determination system only. To distinguish these two calibration systems, the comparative calibration scheme is called Case 1, while the calibration scheme proposed in Sections II and III is called Case 2.

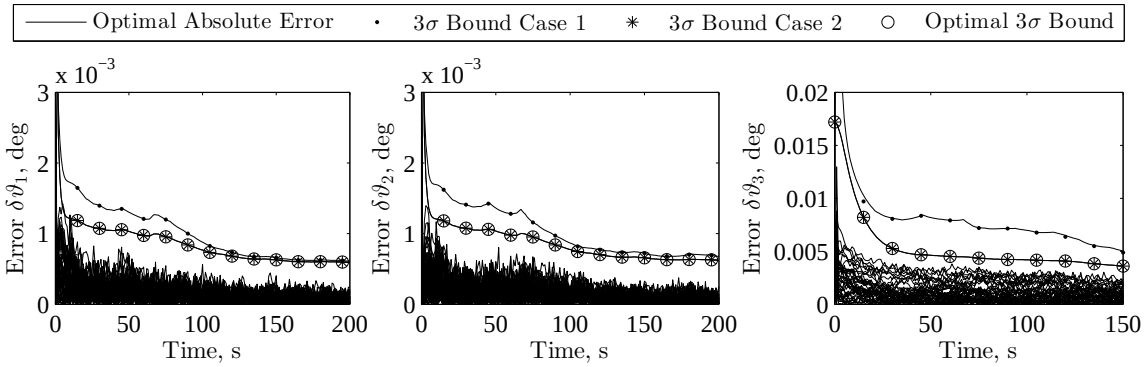

Figure 9. Comparison of 3σ Error Bounds

First, the simulation is performed and the 3σ error bounds of the attitude errors from Cases 1 and 2, and the optimal ones are generated. The absolute estimation errors of the attitude errors from the covariance intersection are also calculated. Comparisons of the attitude errors with their respective 3σ error bounds for 100-time Monte Carlo runs are illustrated in Figure 9. It is seen in this figure that the estimation errors are well bounded. The attitude estimates from Case 1 are less accurate than those from Case 2. Therefore the proposed calibration method can help improve the attitude estimates over those obtained using just the attitude determination system. That is, the use of accelerometers improves the attitude accuracy in addition to using gyros from the attitude determination system. Furthermore, even though the 3σ error bounds from Case 2 are slightly lower than the optimal ones, the differences are negligible. Therefore although the EKF in the calibration system is a suboptimal estimator, the estimation accuracy is very close to the optimal one.

B. Calibration Accuracy Analysis

The calibration errors of the accelerometer biases and corresponding error bounds from Cases 1 and 2 are plotted in Figure 10. Simulation results indicate that the calibration accuracy in both cases is greatly improved using the recalculation process. All the accelerometer biases can be estimated with negligible calibration errors. A fast convergence is also achieved. Therefore the recalculation process is very useful for accelerometer calibration. Furthermore, it is found that the 3σ error bounds of the accelerometer biases from both cases are almost the same. Therefore, the introduction of attitude information cannot improve the accuracy

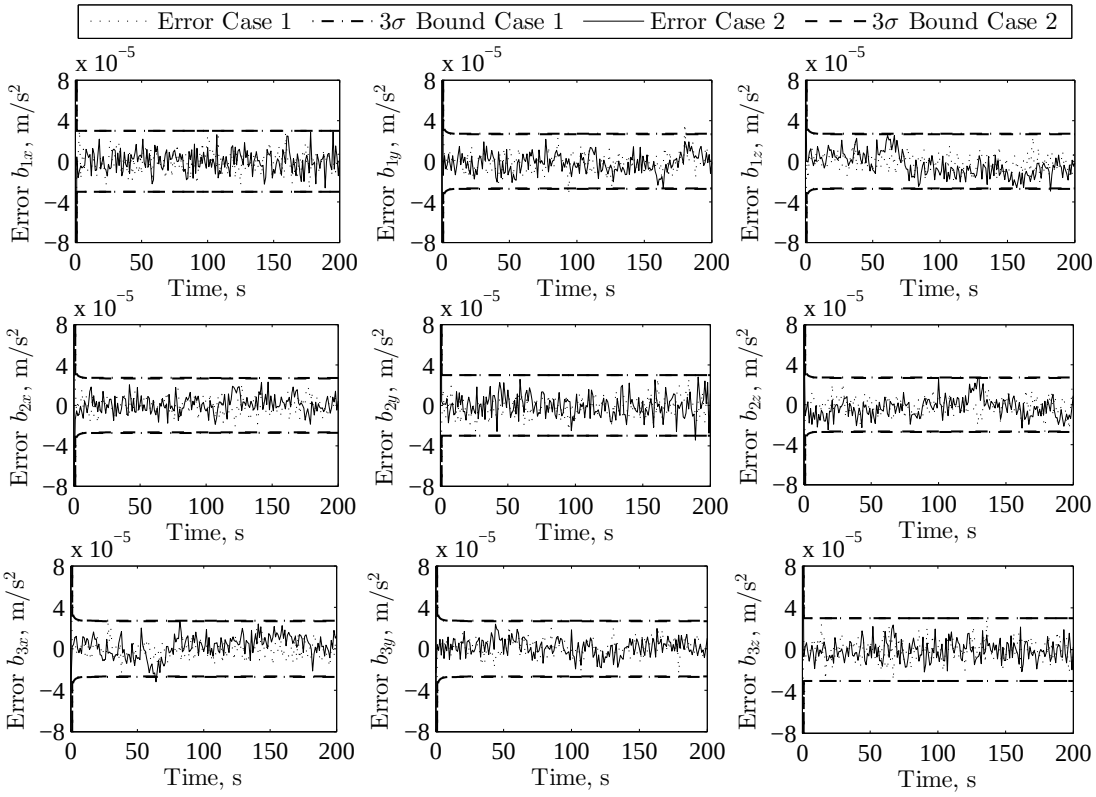

Figure 10. Calibration Errors and 3σ Error Bounds

of the accelerometer bias calibration. However, considering the improvement in the attitude estimates, the proposed calibration method is a better choice. The calibration errors in Figure 10 are based on the single time simulation. In order to show the consistency of the proposed accelerometer calibration approach, an additional 100-time Monte Carlo simulation run is performed. The calibration errors and corresponding 3σ bounds are illustrated in Figure 11. This indicates that consistent estimates are achieved.

It should be mentioned that the calibration method depends on position knowledge of the mass center as well as accurate control of the mass center. This is in fact required for any attitude estimation process that relies on accelerometers, e.g. see Ref. 8. For spacecraft applications, even with a perfect weight report, fuel usage, solar panel flexure, and other relative motions can change the mass center location. It should also be noted that the calibration approach here is not limited to spacecraft applications. Therefore the uncertainty of mass center is not particularly stressed here because often other applications, such as robotic systems, will be less inclined to estimation errors of mass center. Still it is worthy to see how mass center knowledge and other errors affect filter performance.

In order to account for the disturbances in the control acceleration as well as position errors of the mass center, and determine the relationship between the level of disturbance

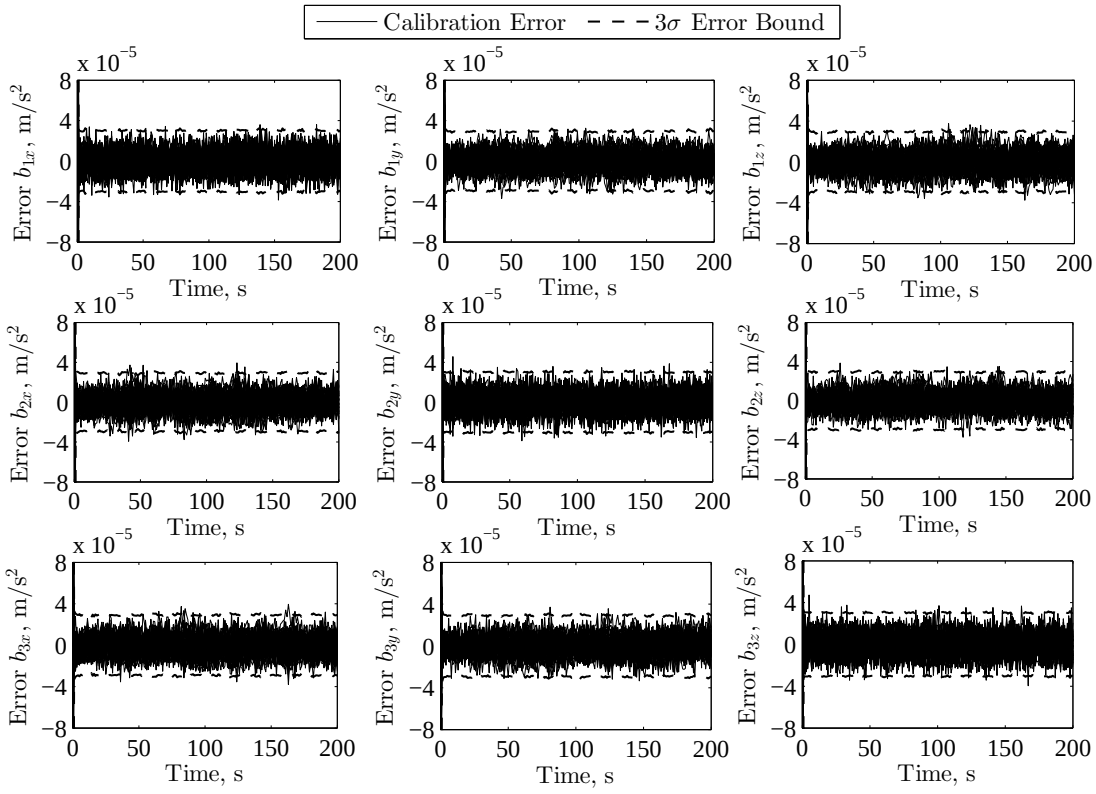

Figure 11. Calibration Errors and 3σ Error Bounds from Monte Carlo Simulations

and the calibration errors, the control acceleration is modeled as the true value plus noise:

$$\boldsymbol{u}_c = \boldsymbol{u}_c^t + \boldsymbol{\eta}_c \tag{65}$$

where $\boldsymbol{u}_c^t$ is the true control acceleration, and $\boldsymbol{\eta}_c$ is the corresponding noise representing the disturbance.

The noise $\boldsymbol{\eta}_c$ is assumed to be a zero-mean Gaussian white-noise process with spectral density $\sigma_c^2 I_3$. Furthermore, in order to account for different noise levels, the following scaling factor is defined:

$$\sigma_c = \gamma \sigma_u \tag{66}$$

The value of γ is separately set to 1, 5 and 10. For each case, the simulation is run 500 times, and the 3σ error bounds of each bias are calculated, which are shown in Figure 12. It can be seen that the disturbance of the control acceleration has a direct impact on the calibration errors. Although the estimation errors of each bias has converged, the error bound increases with the level of disturbance in the control acceleration. This analysis gives a overall understanding of what control acceleration requirements must be in place to ensure good accelerometer bias calibration.

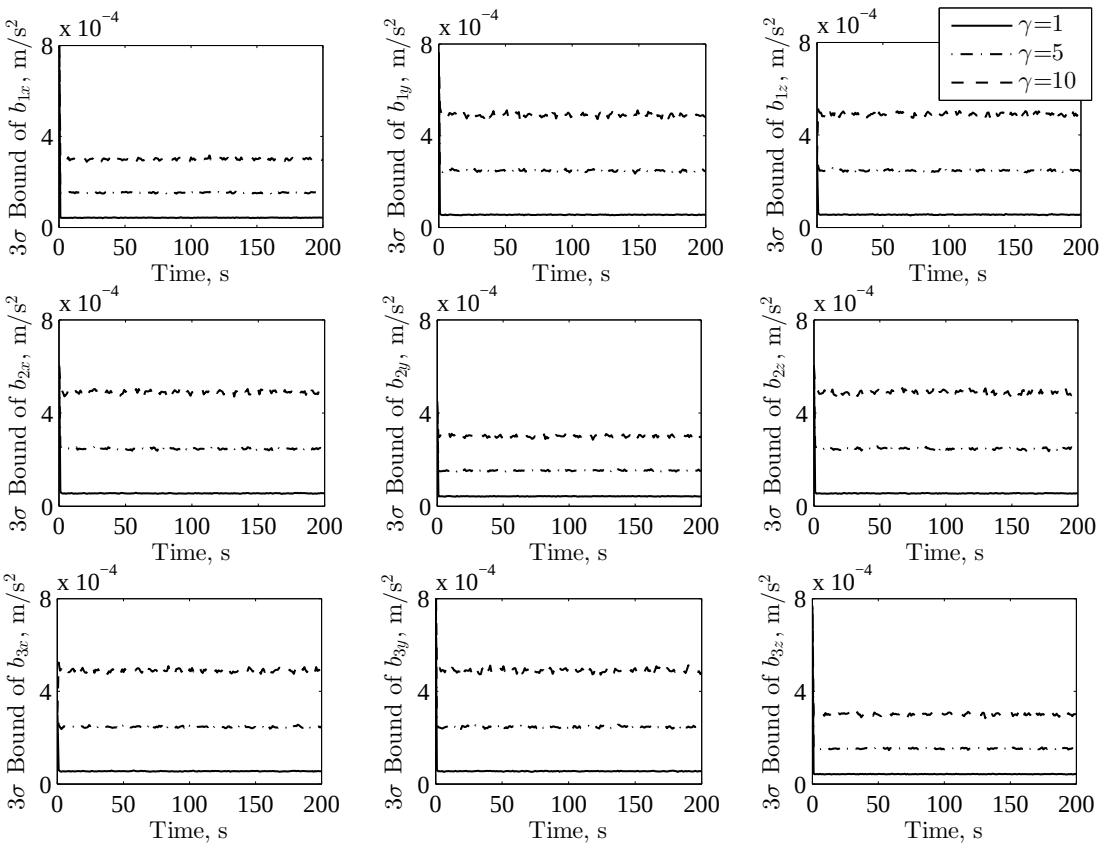

Figure 12. Calibration Errors with Different Levels of Noise

V. Conclusions

This paper investigated a new accelerometer calibration approach when limited or no translational observations is provided. A novel accelerometer calibration method is derived using only attitude and angular velocity information. Because multiple approaches are possible to obtain the angular velocity and attitude information, a general applicability can be achieved. In the algorithm, three accelerometers were used to determine the angular acceleration, which are in turn used to propagate the attitude dynamics and kinematics of the vehicle. Using observations of attitude and angular velocity from the attitude determination system, the attitude, angular velocity and accelerometer biases can be estimated using an extended Kalman filter. Unfortunately, an observability analysis proved that the accelerometer biases are not observable. However, a linear combination of the biases is observable, which can be accurately estimated. This leads to an accurate estimate of the angular acceleration. The recalculation process recalculates the biases with the updated angular velocity and accelerometer biases. The simulation results demonstrated the feasibility and accuracy of the novel calibration approach. Although the estimator is suboptimal, the estimation accuracy

is very close to the optimal estimation using the covariance intersection approach. Improved accuracy in attitude estimation from the original attitude determination system can also be obtained. It is important to note that the approach developed here is not limited to just star trackers. It can work with any attitude sensor system that provides full three-axis attitude determination.

Acknowledgments

The first author would like to thank the support of the National Basic Research Program of China (No. 2012CB720000), the National Natural Science Foundation of China (No. 61374216), and the China Scholarship Council for sponsoring this research.

References

[1]Braun, R. D. and Manning, R. M., "Mars Exploration Entry, Descent, and Landing Challenges," *Journal of Spacecraft and Rockets*, Vol. 44, No. 2, March-April 2007, pp. 310–323, doi:10.2514/1.25116.

[2]Zanetti, R., *Advanced Navigation Algorithms for Precision Landing*, Ph.D. thesis, The University of Texas at Austin, Austin, TX, 2007.

[3]DiNapoli, L. D., *The Measurement of Angular Velocities without the Use of Gyros*, Master's thesis, University of Pennsylvania, Philadelphia, PA, 1965.

[4]Schuler, A. R., Grammatikos, A., and Fegley, K. A., "Measuring Rotational Motion with Linear Accelerometers," *IEEE Transactions on Aerospace and Electronic Systems*, Vol. AES-3, No. 3, May 1967, pp. 465–472, doi:10.1109/TAES.1967.5408811.

[5]Padgaonkar, A. J., Krieger, K. W., and King, A. I., "Measurement of Angular Acceleration of a Rigid Body Using Linear Accelerometers," *Journal of Applied Mechanics*, Vol. 42, No. 3, 1975, pp. 552–556, doi:10.1115/1.3423640.

[6]Liu, I. K., "Discussion: Measurement of Angular Acceleration of a Rigid Body Using Linear Accelerometers," *Journal of Applied Mechanics*, Vol. 43, No. 2, 1976, pp. 377–378, doi:10.1115/1.3423861.

[7]Mital, N. K. and King, A. I., "Computation of Rigid-Body Rotation in Three-Dimensional Space from Body-Fixed Linear Acceleration Measurements," *Journal of Applied Mechanics*, Vol. 46, No. 4, 1979, pp. 925–930, doi: 10.1115/1.3424679.

[8]Chen, J. H., Lee, S. C., and DeBra, D. B., "Gyroscope Free Strapdown Inertial Measurement Unit by Six Linear Accelerometers," *Journal of Guidance, Control, and Dynamics*, Vol. 17, No. 2, March-April 1994, pp. 286–290, doi:10.2514/3.21195.

[9]Parsa, K., Lasky, T. A., and Ravani, B., "Design and Implementation of a Mechatronic, All-Accelerometer Inertial Measurement Unit," *IEEE/ASME Transactions on Mechatronics*, Vol. 12, No. 6, Dec. 2007, pp. 640–650, doi:10.1109/TMECH.2007.910080.

[10]Tan, C. W., Mostov, K., and Varaiya, P., "Feasibility of a Gyroscope-free Inertial Navigation System for Tracking Rigid Body Motion," Tech. Rep. UCB-ITS-PRR-2000-9, Institute of Transportation Studies, University of California, Berkeley, CA, 2000.

[11]Tan, C. W. and Park, S., "Design and Error Analysis of Accelerometer-Based Inertial Navigation

Systems," Tech. Rep. UCB-ITS-PRR-2002-21, Institute of Transportation Studies, University of California, Berkeley, CA, 2002.

[12]Hanson, R. and Pachter, M., "Optimal Gyro-Free IMU Geometry," *AIAA Guidance, Navigation, and Control Conference and Exhibit*, Reston, VA, 2005, AIAA 2005-6151, doi:10.2514/6.2005-6151.

[13]Hung, C. Y. and Lee, S. C., "A Calibration Method for Six-Accelerometer INS," *International Journal of Control, Automation, and Systems*, Vol. 4, No. 5, Oct. 2006, pp. 615–623.

[14]Visser, P. N. A. M., "Exploring the Possibilities for Star-Tracker Assisted Calibration of the Six Individual GOCE Accelerometers," *Journal of Geodesy*, Vol. 82, No. 10, Oct. 2008, pp. 591–600, doi:10.1007/s00190-007-0205-6.

[15]Schopp, P., Klingbeil, L., Peters, C., and Manoli, Y., "Design, Geometry Evaluation, and Calibration of a Gyroscope-Free Inertial Measurement Unit," *Sensors and Actuators A: Physical*, Vol. 162, No. 2, Aug. 2010, pp. 379–387, doi:10.1016/j.sna.2010.01.019.

[16]Markley, F. L. and Crassidis, J. L., *Fundamentals of Spacecraft Attitude Determination and Control*, Springer, New York, NY, 2014, pp. 71, 147, 244–245, 146, 251–252, doi:10.1007/978-1-4939-0802-8.

[17]Shuster, M. D., "A Survey of Attitude Representations," *Journal of the Astronautical Sciences*, Vol. 41, No. 4, Oct.-Dec. 1993, pp. 439–517.

[18]Crassidis, J. L. and Junkins, J. L., *Optimal Estimation of Dynamic Systems, 2nd Edition*, chap. 7, 4, CRC Press, Boca Raton, FL, 2012.

[19]Crassidis, J. L. and Markley, F. L., "Predictive Filtering for Attitude Estimation Without Rate Sensors," *Journal of Guidance, Control, and Dynamics*, Vol. 20, No. 3, May-Jun. 1997, pp. 522–527, doi:10.2514/2.4071.

[20]Crassidis, J. L., "Angular Velocity Determination Directly from Star Tracker Measurements," *Journal of Guidance, Control, and Dynamics*, Vol. 25, No. 6, Nov.-Dec. 2002, pp. 1165–1168, doi:10.2514/2.4999.

[21]Lefferts, E. J., Markley, F. L., and Shuster, M. D., "Kalman Filtering for Spacecraft Attitude Estimation," *Journal of Guidance, Control, and Dynamics*, Vol. 5, No. 5, Sept.-Oct. 1982, pp. 417–429, doi:10.2514/3.56190.

[22]Julier, S. J. and Uhlmann, J. K., "A Non-Divergent Estimation Algorithm in the Presence of Unknown Correlations," *Proceedings of the American Control Conference*, Vol. 4, Albuquerque, NM, June 1997, pp. 2369–2373, doi:10.1109/ACC.1997.609105.

[23]Crassidis, J. L., Cheng, Y., Nebelecky, C. K., and Fosbury, A. M., "Decentralized Attitude Estimation Using a Quaternion Covariance Intersection Approach," *The Journal of the Astronautical Sciences*, Vol. 57, No. 1-2, Jan.-Jun. 2009, pp. 113–128, doi:10.1007/BF03321497.

[24]Markley, F. L., Cheng, Y., Crassidis, J. L., and Oshman, Y., "Averaging Quaternions," *Journal of Guidance, Control, and Dynamics*, Vol. 30, No. 4, Jul.-Aug. 2007, pp. 1193–1196, doi:10.2514/1.28949.